Proceedings of the Twenty-sixth (2016) International Ocean and Polar Engineering Conference **www.isope.org**
Rhodes, Greece, June 26-July 1, 2016

ISBN 978-1-880653-88-3; ISSN 1098-6189

Simulation of a buried pipeline crossing strike-slip fault based on Vector Form Intrinsic Finite Element (VFIFE) method with Fiber element model

Junqing Liu, Leige Xu, Mian Lin
Institute of Mechanics, Chinese Academy of Sciences
Beijing, China

ABSTRACT

The buried pipeline subjected to strike-slip fault would experience large deformation and cause tensile rupture or shear failure of the pipe wall. In order to investigate the mechanism of potential failure position (PFP) of a pipeline, a numerical approach based on the Vector Form Intrinsic Finite Element (VFIFE) method with fiber beam element model (VFIFE-fiber model) is developed. Several key factors, such as geometrical nonlinearity, material nonlinearity, and the interaction between axial force and bending moment are considered. A simple and practicable formula for obtaining the PFP of a pipeline is proposed.

KEY WORDS: buried pipeline; strike-slip fault; soil spring; VFIFE; fiber model; potential failure position of pipe; seismic design

INTRODUCTION

As one of the most important means of transportation of oil and gas, buried pipeline may pass through various complex geological environment. A number of post-earthquake investigations and researches have demonstrated that fault movements probably are the most harmful event for the safety of buried pipeline (Shakib and Zia-Tohidi 2004, Vazouras, Karamanos et al. 2010). This problem has been vastly studied by analytical approach and finite element method (FEM).

In terms of analytical model, pioneering work in the analysis of pipeline subjected to active fault was done by Newmark and Hall (1975). They assumed the pipeline as a cable deforming in straight line. Kennedy, Chow et al. (1977) improved the Newmark-Hall method by considering the soil lateral forces and treating the pipeline deformation near the fault trace as circular arcs. Both Newmark and Kennedy regarded the intersection of the pipeline with the fault trace as the failure position. The methodology developed by Wang and Yeh (1985) is based on dividing the pipeline into four segments, as shown in Fig. 1. Point A is the intersection of the pipeline with the fault trace. Points B and C represent the end of the high curvature zone, while points B′ and C′ are anchorage points at which the axial stress essentially become zero. Segments AB and AC in the high curvature zone on both sides of the fault trace are simplified as circular arcs, in the same way as Kennedy's method, while the other two segments BB′ and CC′ in small deformation zone are treated as beams-on-elastic-foundation. Wang concluded that points A, B and C are probably the dangerous point. Based on the previous work, Karamitros, Bouckovalas et al. (2007) and Trifonov and Cherniy (2010) presented their semi-analytical methodologies, with the assumption that the high curvature zone is treated as elastic beam, instead of circular arcs. They recognized that the maximum strain point along pipeline changes with the increase of fault offset.

In terms of numerical method, Uckan, Akbas et al. (2015) studied buried pipeline at strike-slip fault with intersection angle being equal to 90° by elstoplastic Winkler type springs and pipe element. They concluded that the maximum strain develops at the location near the fault trace. Takada, Hassani et al. (2001) carried out parameter study with shell element model to investigate the deformation of pipeline subjected to strike-slip fault. They concluded that the most unfavorable strain, taking the deformation of the pipe cross-section into consideration, must develop at the start-bending point. Vazouras, Karamanos et al. (2012) used solid element to simulate the surrounding soil and studied the failure mode of buried pipeline at strike-slip fault. Considering local buckling, the curved pipe near the fault trace is prone to damage.

Literature review suggests that the failure position of buried pipeline subjected to strike-slip fault may occur at the intersection of the pipeline with the fault trace or near the fault trace. However the mechanism of the potential failure position (PFP) of a pipeline has not been studied.

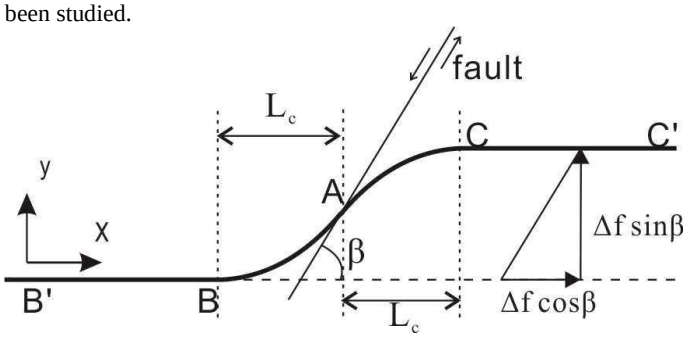

Fig. 1 Schematic representation of fault-induced deformation of pipeline axis

In this paper, the fiber beam element is introduced into the Vector Form Intrinsic Finite Element (VFIFE) method, which has an advantage of handling the problem of geometric nonlinearity. Thus the material nonlinearity, geometric nonlinearity and the interaction between axial force and bending moment are considered. The PFP of buried pipeline subjected strike-slip fault is analyzed, and a simple and practicable formula is proposed.

FIBER BEAM ELEMENT OF VFIFE

The VFIFE method is originally put forward by Ting, Shih et al. (2004). It is proposed for calculating the structural large deformation, large displacement, rigid-body motions and so on. The VFIFE method includes four procedures: (a) definition of particles, (b) discretization of particle path, (c) evaluation of deformations and internal forces, and (d) time integration (Wu, Tsai et al. 2009).

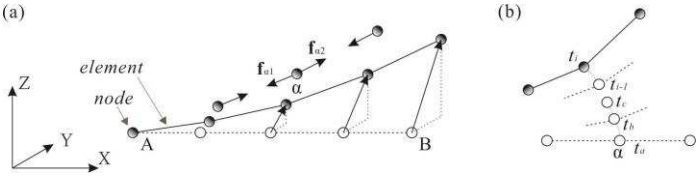

Fig. 2 structure and movement discretization: (a) definition of particles; (b) discretization of particle path

As shown in Fig. 2(a), the structure is composed by particles and element. The mass of the structure is concentrated at the particles, while the elements have no mass but bear internal forces. These positions of particles characterize the shape of the structure. As shown in Fig. 2(b), the structural motion is separated into a series of path elements. Within a path element, the motion of each particle is continuous and satisfies the second Newton's laws.

$$\mathbf{M}_\alpha \frac{\mathrm{d}^2\mathbf{x}_\alpha}{\mathrm{dt}^2}(\mathrm{t}) = \mathbf{P}_\alpha(\mathrm{t}) + \mathbf{f}_\alpha(\mathrm{t}) \qquad (\alpha = 1,2,3,...,\mathrm{N}) \tag{1}$$

Where , $\mathbf{M}_\alpha$ is the mass and mass moment of inertia matrix attached to particle α. $\mathbf{x}_\alpha(\mathrm{t})$ is the position vector of particle α. $\mathbf{P}_\alpha(\mathrm{t})$ is external force, $\mathbf{f}_\alpha(\mathrm{t})$ is internal force. In order to obtain internal forces, the pure deformation of the element should have to be calculated first. Therefore a virtual reverse motion and a set of deformation coordinates are used to calculate the pure deformation. Fig. 3 Shows a two-node 3D beam element with nodal numbers (A, B), moving along an arbitrary path element. Each node has six degrees of freedom. From time t_a to t_b, the increments of nodal translations are $\mathbf{\Delta x}_\mathrm{A}$, $\mathbf{\Delta x}_\mathrm{B}$; and the rotation increments are $\mathbf{\Delta\beta}_\mathrm{A}$, $\mathbf{\Delta\beta}_\mathrm{B}$. As shown in Fig. 4, VFIFE assumes the element undergoes a reverse rigid body motion, including translation $-\Delta\mathbf{x}_\mathrm{A}$, and rotation $-\boldsymbol{\gamma} = -\left(\boldsymbol{\theta}_{\mathbf{ba}} + \mathbf{\Delta\beta}^{\mathbf{A}}_{\hat{\mathbf{x}}}\right)$. In this case, the pure deformation can be obtained. Following the procedure introduced by Ting et al. (2012), a two-node 3D beam element only has six independent variables of deformation displacement, which can be written as

$$\Delta\hat{\mathbf{u}} = \left\{\Delta_\mathrm{e} \quad \Delta\hat{\varphi}_\mathrm{Bx} \quad \Delta\hat{\varphi}_\mathrm{Ay} \quad \Delta\hat{\varphi}_\mathrm{By} \quad \Delta\hat{\varphi}_\mathrm{Az} \quad \Delta\hat{\varphi}_\mathrm{Bz}\right\}^\mathrm{T} \tag{2}$$

Where Δ_e is the axial deformation increment, $\Delta\hat{\varphi}_\mathrm{Bx}$ is torsional deflection, $\Delta\hat{\varphi}_\mathrm{Ay}$ and $\Delta\hat{\varphi}_\mathrm{Az}$ are the bending deformations of node A, $\Delta\hat{\varphi}_\mathrm{By}$ and $\Delta\hat{\varphi}_\mathrm{Bz}$ are the bending deformations of node B. Based on the principle of virtual work, the internal forces can be calculated in a local coordinate system, written as

$$\hat{\mathbf{f}}^* = \hat{\mathbf{f}}_\mathrm{a}^* + \mathbf{\Delta}\hat{\mathbf{f}}^* \tag{3}$$

$$\mathbf{\Delta f}^* = \int_\mathrm{V} \mathbf{B}^\mathrm{T}\mathbf{D}\mathbf{B}\mathbf{\Delta}\hat{\mathbf{u}}\mathrm{dV} \tag{4}$$

where $\mathbf{D}$ is constitutive matrix, $\mathbf{B}$ is strain matrix, written as $\mathbf{B} = \frac{1}{\mathrm{l}^\mathrm{a}}\begin{bmatrix} 1 & 0 & (4-6\mathrm{s})\hat{\mathrm{z}} & (2-6\mathrm{s})\hat{\mathrm{z}} & (4-6\mathrm{s})\hat{\mathrm{y}} & (2-6\mathrm{s})\hat{\mathrm{y}} \\ 0 & \rho & 0 & 0 & 0 & 0 \end{bmatrix}$, $\mathrm{s} = \hat{\mathrm{x}}/\mathrm{l}^\mathrm{a}$, $\rho = \sqrt{\hat{\mathrm{y}}^2 + \hat{\mathrm{z}}^2}$. $\hat{\mathbf{f}}^*$ is the internal force vector at virtual state $\mathrm{A'B'}$; $\hat{\mathbf{f}}_\mathrm{a}^*$ is the internal force vector at time instant t_a; $\mathbf{\Delta}\hat{\mathbf{f}}^*$ is the increment of internal force. When elastic stage of material is considered only, the constitutive matrix is constant, and Eq. 4 has an explicit expression. The increment vector of internal force can be written as

$$\Delta\hat{\mathbf{f}} = \begin{Bmatrix} \Delta\hat{\mathrm{f}}_\mathrm{Ay} \\ \Delta\hat{\mathrm{m}}_\mathrm{Bx} \\ \Delta\hat{\mathrm{m}}_\mathrm{Ay} \\ \Delta\hat{\mathrm{m}}_\mathrm{By} \\ \Delta\hat{\mathrm{m}}_\mathrm{Az} \\ \Delta\hat{\mathrm{m}}_\mathrm{Bz} \end{Bmatrix} = \begin{Bmatrix} \frac{\mathrm{E}^\mathrm{a}\mathrm{A}^\mathrm{a}}{\mathrm{l}^\mathrm{a}}\Delta_\mathrm{e} \\ \frac{\mathrm{G}^\mathrm{a}\hat{\mathrm{I}}^\mathrm{a}_\mathrm{x}}{\mathrm{l}^\mathrm{a}}\Delta\hat{\varphi}_\mathrm{Bx} \\ \frac{\mathrm{E}^\mathrm{a}\hat{\mathrm{I}}^\mathrm{a}_\mathrm{y}}{\mathrm{l}^\mathrm{a}}\left(4\hat{\varphi}_\mathrm{Ay} + 2\hat{\varphi}_\mathrm{By}\right) \\ \frac{\mathrm{E}^\mathrm{a}\hat{\mathrm{I}}^\mathrm{a}_\mathrm{y}}{\mathrm{l}^\mathrm{a}}\left(2\hat{\varphi}_\mathrm{Ay} + 4\hat{\varphi}_\mathrm{By}\right) \\ \frac{\mathrm{E}^\mathrm{a}\hat{\mathrm{I}}^\mathrm{a}_\mathrm{z}}{\mathrm{l}^\mathrm{a}}\left(4\hat{\varphi}_\mathrm{Az} + 2\hat{\varphi}_\mathrm{Bz}\right) \\ \frac{\mathrm{E}^\mathrm{a}\hat{\mathrm{I}}^\mathrm{a}_\mathrm{z}}{\mathrm{l}^\mathrm{a}}\left(2\hat{\varphi}_\mathrm{Az} + 4\hat{\varphi}_\mathrm{Bz}\right) \end{Bmatrix} \tag{5}$$

Here, E_a , A_a , $\hat{\mathrm{I}}^\mathrm{a}_\mathrm{i}\left(\mathrm{i} = \mathrm{x,y,z}\right)$ and l^a are the material tangent modulus, element area, moment of inertia of cross-section and element length at time instant t_a, respectively. Substituting Eq.5 into Eq. 3, we can find that only six components of internal forces of beam element are available. The other six nodal forces can be obtained by the static equilibrium conditions

$$\begin{aligned} &\textstyle\sum \mathrm{F}_{\hat{\mathrm{x}}} = 0, \quad \hat{\mathrm{f}}_\mathrm{Ax} = -\hat{\mathrm{f}}_\mathrm{Bx} \\ &\textstyle\sum \mathrm{M}_{\hat{\mathrm{x}}} = 0, \quad \hat{\mathrm{m}}_\mathrm{Ax} = -\hat{\mathrm{m}}_\mathrm{Bx} \\ &\textstyle\sum \mathrm{M}_{\hat{\mathrm{y}}} = 0, \quad \hat{\mathrm{f}}_\mathrm{By} = -\frac{1}{\mathrm{l}^\mathrm{a}}\left(\hat{\mathrm{m}}_\mathrm{Az} + \hat{\mathrm{m}}_\mathrm{Bz}\right) \\ &\textstyle\sum \mathrm{M}_{\hat{\mathrm{y}}} = 0, \quad \hat{\mathrm{f}}_\mathrm{Bz} = \frac{1}{\mathrm{l}^\mathrm{a}}\left(\hat{\mathrm{m}}_\mathrm{Ay} + \hat{\mathrm{m}}_\mathrm{By}\right) \\ &\textstyle\sum \mathrm{F}_{\hat{\mathrm{y}}} = 0, \quad \hat{\mathrm{f}}_\mathrm{Ay} = -\hat{\mathrm{f}}_\mathrm{By} \\ &\textstyle\sum \mathrm{F}_{\hat{\mathrm{z}}} = 0, \quad \hat{\mathrm{f}}_\mathrm{Az} = -\hat{\mathrm{f}}_\mathrm{Bz} \end{aligned} \tag{6}$$

Thus, the internal nodal forces at both nodes in virtual state $\mathrm{A'B'}$ can be described in local coordinate as

$$\hat{\mathbf{f}}^\mathrm{k} = \begin{bmatrix} \hat{\mathrm{f}}_\mathrm{kx} & \hat{\mathrm{f}}_\mathrm{ky} & \hat{\mathrm{f}}_\mathrm{kz} & \hat{\mathrm{m}}_\mathrm{kx} & \hat{\mathrm{m}}_\mathrm{ky} & \hat{\mathrm{m}}_\mathrm{kz} \end{bmatrix} \quad \mathrm{k} = \mathrm{A,B} \tag{7}$$

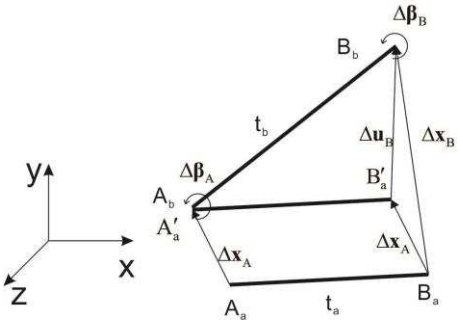

Fig. 3 Nodal displacements of two-node 3D beam element

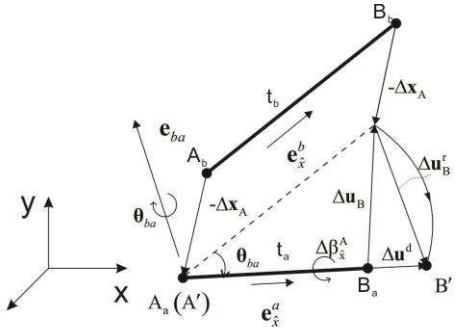

Fig. 4 virtual reverse rigid body motion of an element

After that, have the element do a forward motion, including a translation and a rotation, and return to the original position at time instant t_b. The internal forces at each node are transformed from the local coordinate system to the global coordinate system.

$$\mathbf{f}^{\mathrm{k}} = \begin{bmatrix} \mathbf{R}_{\mathrm{t}}\boldsymbol{\Omega}_{\mathrm{a}}^{\mathrm{T}} & \mathbf{0} \\ \mathbf{0} & \mathbf{R}_{\mathrm{t}}\boldsymbol{\Omega}_{\mathrm{a}}^{\mathrm{T}} \end{bmatrix} \hat{\mathbf{f}}^{\mathrm{k}} \quad \mathrm{k} = \mathrm{A,B} \tag{8}$$

Where $\mathbf{R}_t$ is a 3×3 vector rotation matrix; $\boldsymbol{\Omega}_a^T$ is a 3×3 transition matrix from the global coordinate system to the local coordinate system (Ting et al. 2012). It should be mentioned that the internal forces exerted on the particles are the reactive forces. For an arbitrary particle α, the resultant internal forces are obtained by

$$\mathbf{f}_{\alpha} = -\sum_{\mathrm{i}=1}^{\mathrm{n}} \mathrm{f}^{\mathrm{k}}, \quad \mathrm{k} = \mathrm{A \text{ or } B} \tag{9}$$

Here, n is the number of elements connected with particle α; if particle α is at the starting node of the element, k = A; otherwise, k = B.

In this paper, a simple central difference scheme is adopted to solve the equation of motion of each particle within a path element, i.e. Eq. 1. If the static solution is required, a mass damping force vector $\mathbf{F}_{\alpha}^{\mathrm{dmp}} = -\mu\mathbf{M}_{\alpha}\dfrac{\mathrm{d}\mathbf{x}_{\alpha}}{\mathrm{dt}}$ (μ is the mass damping factor) can be included in Eq. 1. Suppose time incremental step is h, then

$$\mathbf{x}_{\mathrm{n+1}} = \left(\frac{2}{2+\mu\mathrm{h}}\right)\frac{\mathrm{h}^2}{\mathbf{M}_{\alpha}}\left(\mathbf{P}_{\alpha}(\mathrm{t}) + \mathbf{f}_{\alpha}(\mathrm{t})\right) + \left(\frac{4}{2+\mu\mathrm{h}}\right)\mathbf{x}_{\mathrm{n}} - \left(\frac{2-\mu\mathrm{h}}{2+\mu\mathrm{h}}\right)\mathbf{x}_{\mathrm{n-1}} \tag{10}$$

The VFIFE method has been applied to long gas and oil pipelines based on elastic analysis (Xu and Lin 2014, Yuan, Li et al. 2014). To satisfy the needs of piping design, it is necessary to consider the material nonlinearity. Presently, some scholars have considered material nonlinearity in the structural analysis with VFIFE method (Wang, Tsai et al. 2011, Wu, Tsai et al. 2009). In this paper, the fiber beam element model, suitable to account for the interaction between the axial force and bending moment, is adopted. The so-called fiber element is an element divided into several integral points, and the cross section corresponding to each integral point is discretized into fibers, as shown in Figs. 5~6. Hence, the element force-deformation relation is derived by integration of the stress-strain relation of the fibers.

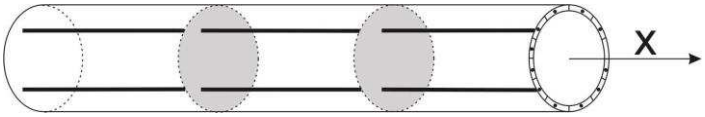

Fig. 5 fiber element, distribution of section in axial

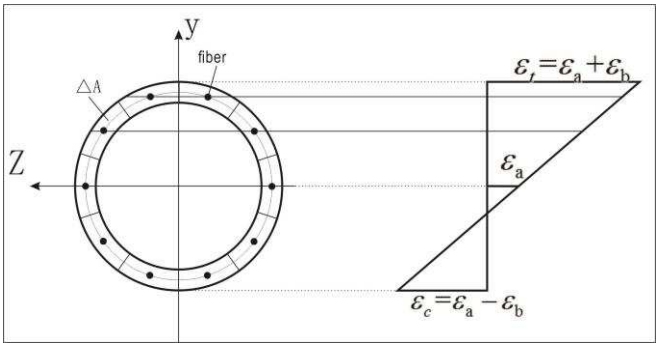

Fig. 6 Section subdivision into fibers and distribution of strain

According to the spatial beam theory, the stress state and strain state at an arbitrary point around cross section can be written as

$$\begin{aligned} \boldsymbol{\sigma} &= \{\sigma_{11} \quad \sigma_{12}\}^{\mathrm{T}} \\ \boldsymbol{\varepsilon} &= \{\varepsilon_{11} \quad \varepsilon_{12}\}^{\mathrm{T}} \end{aligned} \tag{11}$$

where σ_{11} is normal stress caused by axial force and bending movement, σ_{12} is shear stress caused by torque, ε_{11} is normal strain, and ε_{12} is shear strain. The increment strain of fiber can be written as

$$\Delta\hat{\boldsymbol{\varepsilon}} = \mathbf{B}\Delta\hat{\mathbf{u}} \tag{12}$$

when considering the elastic stage of fiber, the stress strain increment relationship obeys Hooke's law.

$$\Delta\hat{\boldsymbol{\sigma}} = \begin{Bmatrix} \Delta\sigma_{11} \\ \Delta\sigma_{12} \end{Bmatrix} = \begin{bmatrix} \mathrm{E} & 0 \\ 0 & \mathrm{G} \end{bmatrix} \begin{Bmatrix} \Delta\varepsilon_{11} \\ \Delta\varepsilon_{12} \end{Bmatrix} = \mathbf{D}_{\mathbf{e}}\Delta\hat{\boldsymbol{\varepsilon}} \tag{13}$$

Where, $\mathbf{D_e}$ is elastic matrix. Otherwise, it is assumed that the material satisfies Von-Mises yield criterion when it turns into plasticity.

$$\mathrm{J}_2 = \frac{1}{3}{\sigma_{11}}^2 + {\sigma_{12}}^2 \tag{14}$$

where, J_2 is the second invariants of the stress deviator. The increment constitutive model for linear isotropic hardening materials can be expressed as

$$\Delta\boldsymbol{\sigma} = \mathbf{D}_{\mathbf{ep}}\Delta\boldsymbol{\varepsilon} = \left(\mathbf{D}_{\mathbf{e}} - \mathbf{D}_{\mathbf{p}}\right)\Delta\boldsymbol{\varepsilon} \tag{15}$$

$$\mathbf{D_p} = \frac{1}{\mu}\begin{bmatrix} E^2\sigma^2 & 3EG\sigma\tau \\ 3EG\sigma\tau & 9G^2\tau^2 \end{bmatrix} \tag{16}$$

where $\mu = E\sigma_{11}^{\ 2} + 9G^2\sigma_{12}^{\ 2} + E_p\left(\sigma_{11}^{\ 2} + 3\sigma_{12}^{\ 2}\right)$, E is elastic Young's modulus, and E_p is plastic Young's modulus. The stress increment of each fiber on beam element is calculated with the different constitutive matrix, judged by elastic deformation stage or ductile deformation stage. The increment of internal force can be calculated by integration of the incremental stress of fibers. Correspondingly, Eq. 4 is written as

$$\begin{aligned} \Delta\hat{\mathbf{f}} &= \int_V \mathbf{B^T}\Delta\hat{\boldsymbol{\sigma}}\mathrm{d}V \\ &= \int_0^1 \begin{bmatrix} \iint_A \Delta\hat{\sigma}_{11}\mathrm{d}A \\ \iint_A \Delta\hat{\sigma}_{12}\rho\mathrm{d}A \\ (4-6s)\iint_A \Delta\hat{\sigma}_{11}\hat{z}\mathrm{d}A \\ (2-6s)\iint_A \Delta\hat{\sigma}_{11}\hat{z}\mathrm{d}A \\ (4-6s)\iint_A \Delta\hat{\sigma}_{11}\hat{y}\mathrm{d}A \\ (2-6s)\iint_A \Delta\hat{\sigma}_{11}\hat{y}\mathrm{d}A \end{bmatrix} \mathrm{d}s = \int_0^1 F(s)\,\mathrm{d}s \end{aligned} \tag{17}$$

where F(s) denotes the integral functions. The Gauss-Lobatto integration scheme, with the advantages of higher computational efficiency, is used in this paper. The increment of internal force is obtained

$$\Delta\hat{\mathbf{f}} = \int_0^1 F(s)\,\mathrm{d}s = \frac{1}{2}\sum_{i=1}^{n} F\left(\frac{1}{2}\xi_i + \frac{1}{2}\right)W_i \tag{18}$$

where n is the number of Gauss-Lobatto integrating point, ξ_i is integration number, and W_i is weight coefficient.

VERIFICATION AND CASE STUDY

In order to validate the accuracy of the VFIFE-fiber model proposed in this paper, a comparison of our results to the results of Karamitros, Bouckovalas et al. (2007) for the strike-slip fault presented here. A typical high-pressure natural gas pipe is considered, with the external diameter D=0.9144m (36 in), wall thickness t=0.0119m (0.469 in). The pipeline steel is of the API5L-X65 type, characterized by a bilinear elasto-plastic stress-strain curve, and the properties are listed in Table 1. The pipeline, with a total length of 1000m, is discretized into 0.5m long VFIFE-fiber element. It is found that the fiber element with n=3 and 24 fibers around the cross section is suitable for obtaining an accurate solution by pilot calculation, and they are selected in the following analysis. It is assumed that the pipeline top is buried under 1.30m of medium-density sand with unit weight γ=18kN/m and friction angle φ=36°. The pipe-soil interaction is described as elastic-perfectly plastic Winkler type spring. The corresponding parameters, listed in Table 2 are calculated according to ALA-ASCE (2001) guidelines. Three intersection angles of β=30°, 45° and 60° are studied. The value of the axial strain at the intersection of the pipeline with the fault trace and the maximum axial, bending, and total longitudinal strain are examined. The results as shown in Fig. 7 indicate that the results calculate by the VFIFE-fiber model agree reasonably to the analytical results, especially with small fault offset. With the increase of fault offset, the error becomes bigger for the reason of the geometric nonlinearity effecting on the pipeline.

Fig. 7 shows that the maximum bending strain ($\varepsilon_{b,max}$) increases at first, and then trends to be stabilized. It is similar for different intersection angles. We can conclude from the comparison with the axial strain at the pipeline-fault trace intersection ($\varepsilon_{a,fault}$), the maximum axial strain ($\varepsilon_{a,max}$) and the maximum total longitudinal strain (ε_{max}) that there exist critical displacements corresponding to them respectively, defined as Δf_a, Δf_b and Δf_c. When the fault offset is greater than the critical displacement, the value of strain increases rapidly. The intersection of the pipeline with the fault trace enters a plastic phase under Δf_a. Δf_b means that $\varepsilon_{a,max}$ develops at the pipeline-fault trace intersection. Δf_c is the demarcation point of tensile and bending. When fault offset is less than Δf_c, bending occupies a leading position in the response of pipeline subjected strike-slip fault, otherwise tension effect take the dominant

Table 1 API5L-X65 steel properties considered in the numerical analyses

Parameter	Value
Yield stress(σ_1)	490 Mpa
Yield strain(ε_1)	0.233%
Elastic Young's modulus(E)	210 Gpa
Plastic Young's modulus(E_ρ)	1.088 Gpa

Table 2 Soil spring properties of medium-density sand

Direction	Yield force (kN/m)	Yield displacement (mm)
Axial	40.5	3.0
Transverse horizontal	318.6	11.4
Vertical upward	52.0	2.2
Vertical downward	1360.0	100.0

Table 3 Soil spring properties of loose sand

Direction	Yield force (kN/m)	Yield displacement (mm)
Axial	40.5	3.0
Transverse horizontal	318.6	11.4
Vertical upward	52.0	2.2
Vertical downward	1360.0	100.0

Table 4 Soil spring properties of dense sand

Direction	Yield force (kN/m)	Yield displacement (mm)
Axial	40.5	3.0
Transverse horizontal	318.6	11.4
Vertical upward	52.0	2.2
Vertical downward	1360.0	100.0

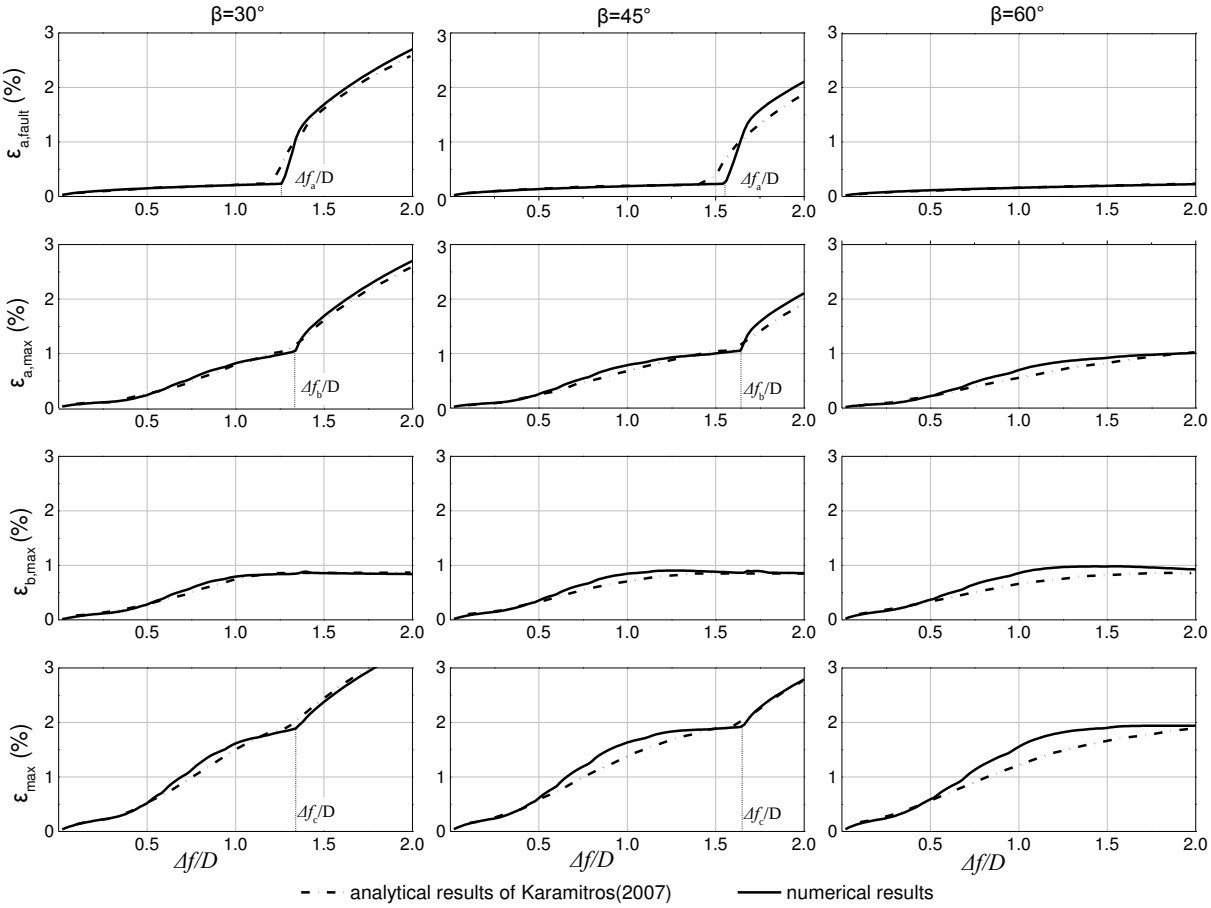

Fig. 7 Comparison of the results of the VFIFE-fiber model to the results of Karamitros (2007)

place. Fig. 7 also shows that the critical displacements all increase with the intersection angle. For β=60°, bending dominates the deformation of pipeline throughout the fault offset varying from 0 to 2D. For β=30°, Δf_a=1.26D，Δf_b=1.34D and Δf_c=1.36D, and the relationship of critical displacements can be obtained as follows:

$$\Delta f_a < \Delta f_b \approx \Delta f_c \tag{19}$$

It is well known that the PFP of the pipeline at which the maximum total strain develops, lies in high curvature zone near the fault. The numerical results show that the deformation mechanism of pipe near the fault trace is complex. The pipeline is easily suffered from the shear failure in the maximum curvature zone, or tensile rupture at the pipeline-fault trace intersection.

A study was carried out to investigate the PFP of a pipeline with three intersection angles as mentioned above, and three granular backfills: loose, medium dense and dense sand. The soil-spring properties for loose and dense sand are listed in Table 3 and Table 4, respectively. For purposes of comparison, the results of the analysis have been summarized in the same diagram, which shows the variation of the pipeline curved length (L_c), the location of maximum bending strain, maximum axial strain and total longitudinal strain with respect to the fault offset. As shown in Fig. 8, the location of maximum bending strain $x_{b,max}$, increases slowly at first, and then trends to be stabilized, meanwhile the pipeline curved length is still growing. Because of flexure effects, it may appear that the location of maximum axial strain $x_{a,max}$ is equivalent to $x_{b,max}$. Under the joint action of tension and bending, the position of total longitudinal strain could be divided into three phases: Ⅰ, Ⅱ and Ⅲ. There exist $x_{max}=x_{b,max}$ both in phases Ⅰ and Ⅱ, nonetheless the value of x_{max} increases slowly in the former phase, and trends to be stabilized in the latter one. In phase Ⅲ the value of x_{max} is about 1m, which means total longitudinal strain is located near the fault. We can image that, x_{max} will be equivalent to 0 with the increase of fault offset. In essence, phase Ⅰ indicates the beam bending behavior while phase Ⅲ indicates the cable behavior. Considering the comprehensive influence of the beam and cable behavior, phase Ⅱ can be defined as a transitional stage. The demarcation point between phases Ⅱ and Ⅲ is corresponding to Δf_c.

Fig. 8 also shows that, when the results are compared at a constant magnitude of Δf for various intersection angels under the same granular backfill, x_{max}, as well as Δf_c, increase as the intersection angle increased from 30-60°. For the constant magnitude of Δf and β, both x_{max} and Δf_c decrease as the compactness of granular backfill increased.

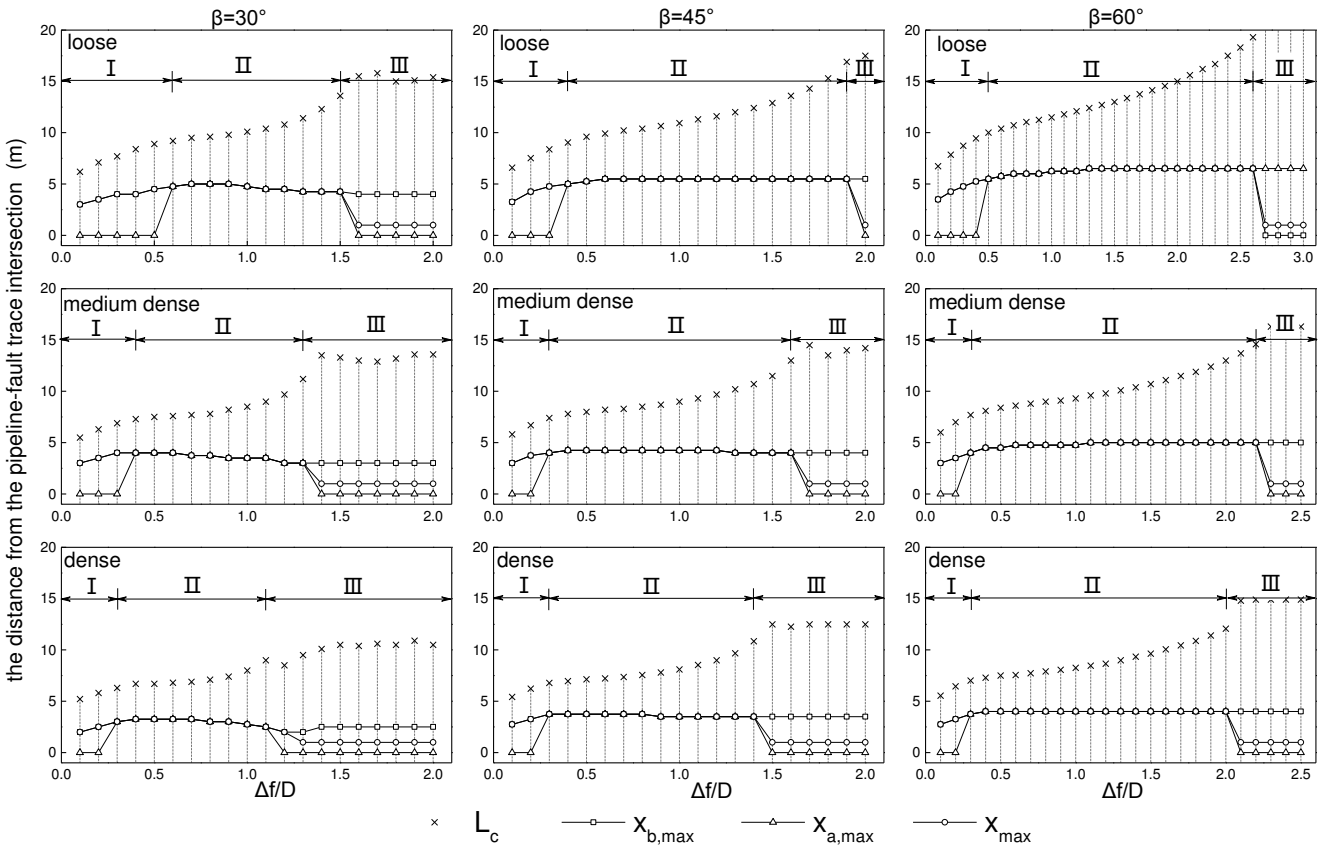

Fig. 8 The distance from the pipeline-fault trace intersection versus fault offset

PROPOSED FORMULA FOR PFP OF A PIPELINE

In general, the response of buried pipeline subjected to strike-slip fault is complex due to the combined influence of beam and cable behavior, which affect the PFP of a pipeline. Considering the less strain in phase Ⅰ, the rising stage of x_{max} has been ignored. For the sake of simplicity, the maximum strain can be supposed to develop at the pipeline-fault trace intersection. Hence, a simple and practicable formula for calculating PFP for the design of buried pipeline crossing strike-slip is proposed.

$$x_{max} = 0.424\left(\frac{318.6}{q_u}\right)^{\frac{1}{4}}\left(\frac{EI}{q_u}\right)^{\frac{1}{3}}\sin\beta, \Delta f < \Delta f_c$$
$$x_{max} = 0, \Delta f \geq \Delta f_c \quad (20)$$

where, E is the elastic modulus; q_u is the maximum lateral soil force per unit length, according to the ALA-ASCE (2001); $\left(\frac{318.6}{q_u}\right)^{\frac{1}{4}}$ is dimensionless factor taking the effect of backfill type into consideration, and the datum value 318.6 kN/m is the maximum lateral soil force of medium-dense sand; Δf_c is the demarcation point between phases Ⅱ and Ⅲ, associated with β, property of pipe material and backfill. It can be obtained from the above analysis that Δf_c is greater than Δf_a. Following to the method for calculating the axial force at the intersection of the pipeline with the fault trace used by analytical approaches, the fault offset corresponding to the axial stress equal to the yield limit σ_1 is obtained:

$$\Delta f_a' = \frac{\sigma_1^2 A}{E t_u \cos\beta} \quad (21)$$

Here, A is the area of pipe cross-section, and t_u is the maximum friction per unit length of pipe. The results of relative fault offset $\Delta f_a'/D$ based on Eq. 21 and the results of numerical for $\Delta f_c/D$ are shown in Table 5, with the different intersection angles and backfill types considered. Due to neglecting the effect of bending on pipe elongation in analytical method, there are great error between $\Delta f_a'/D$ and $\Delta f_c/D$. Table 5 also shows that the error is correlative with the properties of backfill. Therefor the critical displacements Δf_c is written as:

$$\Delta f_c = \left(0.9955 + \frac{4.225 q_u}{10^7}\right)\frac{\sigma_1^2 A}{E t_u \cos\beta} \quad (22)$$

The results predicted by Eq. 20 and 22 are compared to the numerical results, with intersection angel β=50° and three backfill types considered. As shown in Fig. 9, the overall results are satisfactory, which indicates the proposed formula for calculating the position of pipe potential failure is viable with the intersection angle varying from 30° to 60°. When the intersection angle is larger than 60°, the phase Ⅲ of x_{max} may not appear, due to a higher effect of bending on the buried pipeline.

Table 5 Comparison of $\Delta f_a'/D$ and $\Delta f_c/D$

Backfill type	β	$\Delta f_a'/D$	$\Delta f_c/D$	error
loose	30°	1.45	1.58	0.08966
	45°	1.78	1.92	0.07865
	60°	2.52	2.7	0.07143
medium dense	30°	1.2	1.36	0.13333
	45°	1.47	1.66	0.12925
	60°	2.08	2.3	0.10577
dense	30°	1.04	1.24	0.19231
	45°	1.27	1.48	0.16535
	60°	1.79	2.1	0.17318

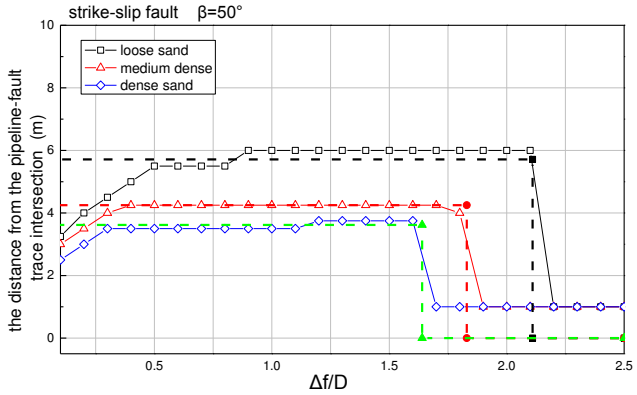

Fig. 9 Comparison of the results of the proposed formula to the numerical results

SUMMARY

The main purpose of this paper is to investigate the PFP of a pipeline subjected to strike-slip fault. The Vector Form Intrinsic Finite Element (VFIFE) method with fiber beam element model is used. It is demonstrated that the present VFIFE-fiber model is effective in computing structural responses with large geometric and material nonlinearities by comparing the results of the present VFIFE-fiber model and the results of analytical method in literature for buried pipeline crossing strike-slip fault. The mechanism of the PFP of a pipeline is studied, and the simple and practicable formulas for x_{max} and Δf_c are proposed. The main conclusions have been achieved:

The PFP of a pipeline could be divided into three phases: Ⅰ, Ⅱ and Ⅲ. Phase Ⅰ indicates the beam bending behavior, and x_{max} increases with the fault offset, as well as the pipeline curved length. Phase Ⅱ can be defined as a transitional stage, and x_{max} trends to be stabilized. Phase Ⅲ indicates the cable behavior, and x_{max} is about 1m.

When fault offset is larger than the critical displacement Δf_c as the demarcation point between phases Ⅱ and Ⅲ, tension effect occupies a leading position in the behavior of pipeline subjected strike-slip fault. Hence the pipeline will be suffered from tensile rupture.

Both the position of pipe potential failure x_{max} and the critical displacement Δf_c increase as the intersection angle increased from 30-60°, decrease as the compactness of granular backfill increased.

ACKNOWLEDGEMENTS

This research was financially supported by the National High-tech R&D Program of China (No. 2006AA09Z301).

REFERENCES

Alliance Lifelines Alliance. (2001). Guidelines for the design of buried steel pipe. American Society of Civil Engineers..

Karamitros D K, Bouckovalas G D, Kouretzis G P. (2007). "Stress analysis of buried steel pipelines at strike-slip fault crossings." Soil Dynamics and Earthquake Engineering 27(3): 200-211.

Kennedy R P, Chow A M, Williamson R A. (1977). "Fault movement effects on buried oil pipeline." Transportation engineering journal of the American Society of Civil Engineers 103(5): 617-633.

Newmark N M, W J Hall (1975). "Pipeline design to resist large fault displacement." In: proceedings of the U.S. national conference on earthquake engineering, Ann Arbor, University of Michigan, 416-25

Shakib H, R Zia-Tohidi (2004). "Response of steel buried pipelines to three-dimensional fault movements by considering material and geometrical non-linearities." Proceedings of the 13th World Conference on Earthquake Engineering, Vancouver, BC, Canada.

Takada S, Hassani N, Fukuda K. A. (2001). "A new proposal for simplified design of buried steel pipes crossing active faults." Earthquake engineering & structural dynamics 30(8): 1243-1257.

Ting E C, Shih C, Wang Y K. (2004). "Fundamentals of a vector form intrinsic finite element: Part I. Basic procedure and a plane frame element." Journal of Mechanics 20(02): 113-122.

Ting E C, Duan Y F and Wu D Y. (2012). "Fundamentals of a vector form intrinsic finite element: Part I. Basic procedure and a plane frame element." Vector Mechanics of Structures, Science Press. (In Chinese)

Trifonov O V, and V P Cherniy (2010). "A semi-analytical approach to a nonlinear stress–strain analysis of buried steel pipelines crossing active faults." Soil Dynamics and Earthquake Engineering 30(11): 1298-1308.

Uckan E, Akbas B, Shen J, et al. (2015). "A simplified analysis model for determining the seismic response of buried steel pipes at strike-slip fault crossings." Soil Dynamics and Earthquake Engineering 75: 55-65.

Vazouras P, Karamanos S A, Dakoulas P. (2010). "Finite element analysis of buried steel pipelines under strike-slip fault displacements." Soil Dynamics and Earthquake Engineering 30(11): 1361-1376.

Vazouras P, Karamanos S A, Dakoulas P. (2012). "Mechanical behavior of buried steel pipes crossing active strike-slip faults." Soil Dynamics and Earthquake Engineering 41: 164-180.

Wang L R L, Yeh Y H (1985). "A refined seismic analysis and design of buried pipeline for fault movement." Earthquake engineering & structural dynamics 13(1): 75-96.

Wang R Z, Tsai K C, Lin B Z. (2011). "Extremely large displacement dynamic analysis of elastic–plastic plane frames." Earthquake engineering & structural dynamics 40(13): 1515-1533.

Wu T Y, Tsai W C, Lee J J. (2009). Dynamic elastic–plastic and large deflection analyses of frame structures using motion analysis of structures. Thin-Walled Structures, 47(11), 1177-1190.

Xu L, Lin M (2014). "Integrate Pipe-Soil Interaction Model with the Vector Form Intrinsic Finite Element Method-Nonlinear Analysis of Free-Span." The Twenty-fourth International Ocean and Polar Engineering Conference, International Society of Offshore and Polar Engineers.

Yuan F, Li L, Guo Z, et al. (2014). "Landslide Impact on Submarine Pipelines: Analytical and Numerical Analysis." Journal of Engineering Mechanics 141(2): 04014109.